Carbon Trends 23 (2026) 100618

Contents lists available at ScienceDirect

Carbon Trends

journal homepage: www.elsevier.com/locate/cartre

Thiourea modification of fluorescent nanodiamonds towards enhanced quantum sensing

Péter Rózsa [a,b], Olga Krafcsik [c,d], Sándor Lenk [c], David Beke [b,e], Adam Gali [b,c,f,*]

[a] Hevesy György PhD School of Chemistry, Eötvös Loránd University, Pázmány Péter sétány 1/A, H-1117 Budapest, Hungary
[b] HUN-REN Wigner Research Centre for Physics, Institute for Solid State Physics and Optics, P.O. Box 49, H-1525 Budapest, Hungary
[c] Department of Atomic Physics, Institute of Physics, Budapest University of Technology and Economics, Műegyetem rkp. 3., H-1111 Budapest, Hungary
[d] HUN-REN Centre for Energy Research, Institute of Technical Physics and Materials Science, P.O. Box 49, H-1525 Budapest, Hungary
[e] Kandó Kálmán Faculty of Electrical Engineering, Óbuda University,Bécsi út 94-96, H-1034 Budapest, Hungary
[f] MTA-WFK Lendület "Momentum" Semiconductor Nanoparticles Research Group, P.O. Box 49, H-1525 Budapest, Hungary

ARTICLE INFO

Keywords:
Nanodiamond
High pressure-high-temperature
Thiourea
Thiolation
oxidation
Fluorescent
Nitrogen-vacancy center
Zeta-potential

ABSTRACT

We functionalized fluorescent nanodiamonds of various sizes using a thiourea-based thiolation reaction to tailor their surface chemistry for biological and quantum technological applications. Spectroscopic analyses revealed that this reaction generates a complex mixture of sulfur- and nitrogen-containing groups, arising from the reaction of thiourea with surface functional groups and from oxidative cyclization. Since the charge stability of negatively charged nitrogen-vacancy (NV^-) centers is strongly influenced by the near-surface electronic structure, surface modifications that enhance this stability—while preserving colloidal dispersibility and enabling further functionalization—are essential for quantum sensing applications. We show that the surface chemistry produced through the reaction of nanodiamonds with thiourea increases electron availability and favors the stabilization of the NV^- charge state. These results highlight the potential of thiourea-derived surface modification as an effective route to improve the quantum performance of nanodiamonds.

1. Introduction

Fluorescent nanodiamonds (FNDs) consisting of nitrogen-vacancy (NV) centers have attracted significant attention over the last decades due to their long-term biocompatibility and photostability [1,2], low toxicity [3,4], single-photon emission properties [5], high sensitivity to local magnetic [6,7], electric [8], and strain [9] fields, and temperature [10–14], as well as their suitability for single particle tracking [15,16], and long-term imaging [17–19]. The NV center is one of the most well-known point defects in diamond, consisting of a substitutional nitrogen atom adjacent to a missing carbon atom (vacancy) in the diamond lattice. Nitrogen-vacancy defects can exist in two charged states: neutral (NV^0, S = 1/2) and negatively charged (NV^-, S = 1), in which the negative charge state is typically donated by other substitutional nitrogen defects. The negatively charged state is the most relevant for quantum technological applications [20]. However, in the case of nanodiamonds, stabilizing NV^- remains challenging, as NV centers become shallow defects and surface states can act as sources of holes under illumination [21], or shift the Fermi level, making electron depletion at shallow NV centers energetically favorable. Adsorbed electrolyte species and fluctuating surface dipoles also aggravate charge instability [22]. Surface engineering of nanodiamonds is therefore essential to suppress these destabilizing pathways, shift the near-surface Fermi level upward, and reliably maintain the NV^- charge state required for quantum sensing applications.

Nanodiamond surfaces are rich in functional groups, such as C=O, COOH, epoxy groups, and modifying these surfaces is a common strategy to tailor their properties for specific applications [23–26]. Several studies have investigated the effect of different surface groups on NV centers. Surface groups with positive electron affinity, such as certain oxygen groups [27–31], nitrogen [32–34] and fluorine groups [35,36] can stabilize the shallow NV centers. In contrast, surface groups with negative electron affinity, such as hydrogen [37] and silicon [34], tend to destabilize the shallow NV^- centers. Thiol groups exhibit diverse chemistry, including cross-linking through sulfide or disulfide formation [38], click chemistry in various reaction media [39], self-assembled

* Corresponding author.
E-mail address: gali.adam@wigner.hun-ren.hu (A. Gali).

https://doi.org/10.1016/j.cartre.2026.100618
Received 9 December 2025; Received in revised form 22 January 2026; Accepted 23 January 2026
Available online 24 January 2026

monolayers (SAMs) [40], heavy metal scavenging [41], biosensing [42], biomedical applications [43]. and the passivation and stabilization of noble metal nanoparticles for biological applications [44]. Indeed, thiol functionalization of FNDs has been proposed as a useful strategy for quantum sensing, i.e., for immobilization on metallic surfaces [45], and especially for biological applications due to the rich variation of standard binding protocols for thiols [45–48]. It is surprising, therefore, that no direct thiol functionalization of NV containing diamond surface has been reported so far. However, the effect of thiol groups on pH sensing has been demonstrated by surface-modified FNDs with a polycysteine layer [49]. Even though, thiolation of diamonds has been reported in the literature [50–52], none of these studies has investigated the impact of surface modification on the fundamental properties of NV centers in FNDs. Theoretical studies, on the other hand, predicted an unfavorable effect from thiol groups [47].

While the presence of thiol groups, particularly a uniform thiol termination, might destabilize the shallow NV^- centers, recent studies showed that the heterogeneity of surface chemistry, i.e., amine termination in the presence of oxygen-containing surface moieties [53,54], can enhance NV^- stability, despite the amine also being considered unfavorable. In fact, even the sp^2 carbon species have been shown to be useful for charge stabilization under specific conditions [55–57].

One of the primary methods for introducing thiol groups involves the use of thiourea. Under normal thiourea-mediated thiolation conditions [50,51], hydroxyl groups are first converted into alkyl halides, after which thiourea undergoes nucleophilic substitution to form surface-bound isothiouronium intermediates. These intermediates are subsequently cleaved under alkaline conditions to yield thiol-functionalized organic compounds. In the presence of other functional groups, excess thiourea and under oxidative or strongly acidic–basic conditions, however, thiourea can undergo many different reactions, and even cyclization reactions [58,59], producing reactive intermediates such as formamidine disulfide, cyanamide, and dicyandiamide, which may further condense into various dimeric, oligomeric, or cyclic sulfur- and nitrogen-containing species.

In this work, we applied a thiourea-based surface modification to nanodiamonds of various sizes in order to enhance their chemical functionality while preserving their optical performance. We show that the proposed reaction produces not only thiol groups, which are useful for subsequent biofunctionalization and quantum-sensing interfaces, but also sulfur- and nitrogen-containing conjugated cyclic species arising from thiourea cyclic oxidation. These additional surface functionalities create an optimized electronic environment that stabilizes the negatively charged NV^- state, even for the smallest 20 nm nanodiamonds, without compromising colloidal stability, demonstrating that the thiourea-derived surface chemistry provides an effective route to increase both the functional versatility and quantum performance of nanodiamonds.

2. Materials and methods

2.1. Materials

All materials were used as received, without purification. Ammonia solution (28% GPR Rectapur, VWR Chemicals), $NaBH_4$ (>98% powder, Sigma Aldrich), Hydrogen bromide (HBr) (48%, Acros Argonics), Acetic acid (HOAc) (96%, Reanal), thiourea (Reanal), NaOH (Reanal Normapur, pellets, Sigma Aldrich), H_2SO_4 (95%, Normapur, VWR Chemicals), and HPHT fluorescent nanodiamonds from Adámas Nanotechnology, USA (20, 30, 40, 50, 100, 140 nm nominal diameter) containing high concentrations of NV centers.

2.2. Instruments and characterization

Fourier Transform Infrared Spectroscopy (FTIR) measurements were conducted using a Bruker IFS 66v/S spectrometer operated at 3 mbar pressure, equipped with a Globar source and a liquid-nitrogen-cooled MCT (mercury-cadmium-telluride) detector. The samples were drop-cast onto a single-side polished <100> Si wafer.

The X-ray photoelectron spectroscopy (XPS) analyses were performed with an Escalab xi+ (ThermoFisher) using a monochromatic Al Kα source. A charge neutralizer was applied to all specimens. The analyzed area had a diameter of 650 microns. The instrument base pressure was 3×10^{-10} mbar. The samples were drop-cast onto a Nb substrate (GoodFellow GmbH, Hamburg, Germany). All spectra were calibrated using the Nb $3d_{5/2}$ orbital of Nb_2O_5 at 207.1 eV and the C 1s peak of adventitious carbon (C-C/C-H) at 284.8 eV. For the S 2p orbital, a ratio of 1:2 (S $2p_{1/2}$:S $2p_{3/2}$) and an energy separation of 1.2 eV were used as split parameters. Spectra were analyzed with CasaXPS software (version 2.3.23). The peaks were fitted with a GL30 (Gaussian/Lorentzian) function with 30% Lorentzian character, and Shirley-type background subtraction was applied.

Zeta potential measurements were performed using a Zetasizer Nano Z (Malvern Instruments, UK). Sample concentrations were approximately 10^{-3} mg/mL, with the temperature maintained at 23°C. The viscosity of water was set to 0.8872 cP, and the refractive index and the absorbance of FND were set to 2.42 and 0, respectively. DTS1070 type specialized cuvettes were used, and at least 5 replicates were measured for each sample.

Photoluminescence (PL) measurements were conducted using a Renishaw inVia Raman Microscope equipped with a 50 × Leica objective and a Nd:YAG laser at 532 nm. FND samples were drop-cast onto single-sided polished <100> silicon wafers. PL spectra were collected from aggregated nanodiamonds. At least seven different points on each sample were measured. The incident laser power was kept low (~ 36 μW) to prevent charge-state conversion of the NV centers.

The fractions of neutral and negatively charged NV centers were calculated based on the assumption that the overall spectrum is a linear combination of the pure NV^0 and NV^- spectra with appropriate weighting factors. The Levenberg-Marquardt (LM) algorithm was used for iterative fitting [60–62].

The Raman measurements were performed using multimodal laser excitation on a Renishaw inVia Raman Microscope, employing a He-Cd laser at 325 nm and a diode laser at 785 nm. FND samples were drop-cast onto single-side polished <100> silicon wafer, and spectra were collected from aggregated nanodiamonds from 9 different points on each sample.

2.3. Synthesis of surface-modified FNDs

The thiourea-modified FNDs were synthesized following a modified protocol [50,51]. First, 1 mL of a 1 mg/mL dispersion of as-received Adámas HPHT FNDs (hereafter referred to as ND-COOH) was diluted to 10 mL and adjusted to pH 14 by adding a few drops of 25% NH_3 solution. Subsequently, 80 mg $NaBH_4$ was added, and the mixture was stirred at 70°C for 12 h to reduce surface carboxyl groups, yielding hydroxyl-terminated nanodiamonds (ND-OH). To prepare the surface-modified nanodiamond sample (ND-SH), ND-OH was evaporated to dryness in a 25 mL round-bottom flask, redispersed in 3 mL of a HBr:HOAc mixture (1:2 by volume), and 0.11 g thiourea was added. The suspension was ultrasonicated at 80°C for 3 h. Afterward, 6 mL of ice-cooled 7.5 M NaOH was added to the hot mixture, and the reaction was stirred for an additional 12 h at room temperature. The resulting dispersion was acidified with concentrated H_2SO_4 (96%) to pH 1–2 and purified using a 1 kDa Macrosep centrifugal filter until the permeate conductivity reached 0 μS (Fig. 1).

3. Results and discussion

Surface modification in general alters the chemical composition and modifies the surface charge distribution, acid–base properties, and ionization behavior. The zeta-potential of ND-COOH fell within a

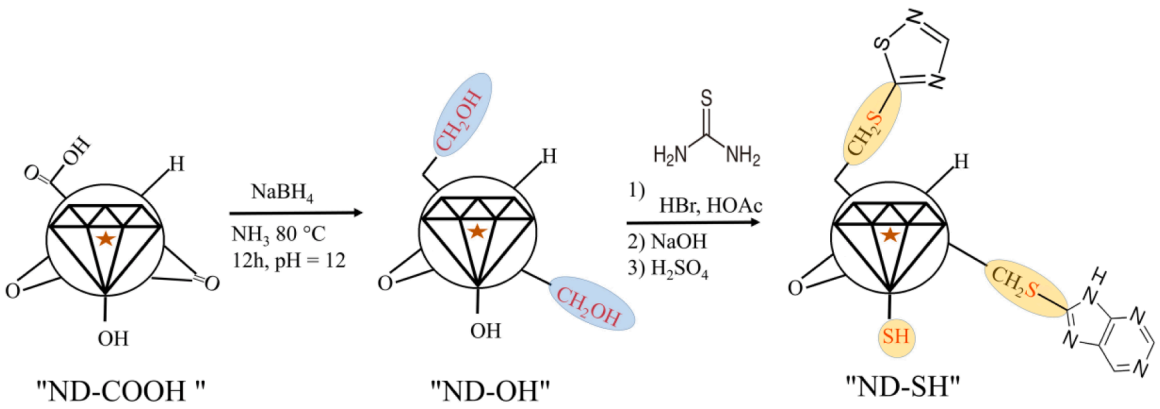

Fig. 1. Synthesis of thiourea-modified FNDs.

narrow range of [−30; −40 mV] (Fig. 2 and Table 1). After surface modification, the zeta-potential of the nanodiamonds decreased to [−25; −10 mV].

The removal of highly ionized carboxyl groups, the introduction of less ionizable thiol moieties, and the formation of oxidized sulfur and C–N species all can shift the zeta potential toward less negative values relative to ND-COOH [,63,64]. as indeed observed.

Fig. 3 compares the FTIR spectra of the ND20-COOH and ND20-SH samples. The ND20-COOH spectrum was dominated by oxygen-containing surface groups, including C–O vibrations near ~1100 cm^{-1}, a broad O–H band at ~3200 cm^{-1}, and carboxyl-related features between 1600–1700 cm^{-1}. Following the surface modification, the intensities of the C=O and COOH bands decreased while the O-H bands increased. The observed increase in the OH-related bands may in principle arise from either surface-adsorbed water or from the intended surface modification. Although adsorbed water cannot be completely eliminated, its contribution is expected to be minor under the applied low-pressure and inert-atmosphere FTIR measurement conditions. We therefore attribute the dominant contribution to the enhanced OH signal to the surface modification of the nanodiamonds.

Although characteristic S–H, C–S, and S–S vibrations are expected to appear in the 600–900 cm^{-1} region, these modes are inherently weak and further obscured by the strong diamond–related and C–O/C–H bands, rendering them undetectable in both FTIR and Raman spectra [65]. Instead, the most notable spectral change is a broadening of the bands between 1000–1200 cm^{-1} and 1250–1550 cm^{-1}, a region that can

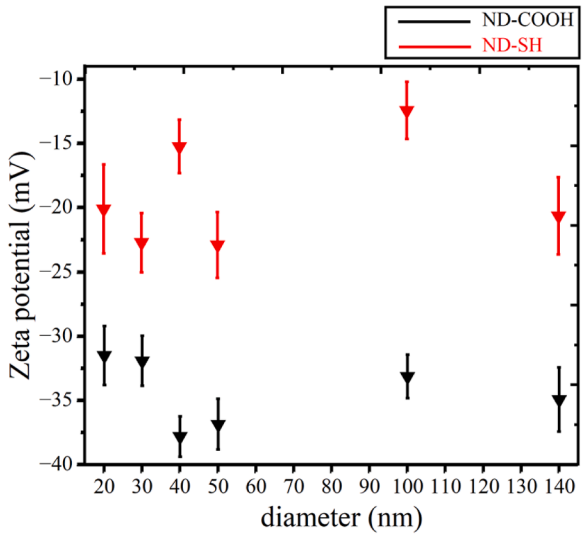

Fig. 2. Zeta-potential of ND-COOH and ND-SH samples.

Table 1
Zeta-potential values of ND-COOH, ND-SH samples and their statistical parameters.

Size (nm)	ND-COOH Mean (SD) (mV)	ND-SH Mean (SD) (mV)
20	−31.5 (2.3)	−20.2 (3.5)
30	-32.0 (2.0)	−22.8 (2.3)
40	−37.8 1.6)	−15.3 (2.1)
50	−36.9 (2)	−23.0 (2.5)
100	−33.2 (1.7)	−12.5 (2.2)
140	−35.0 (2.5)	−20.7 (3.0)

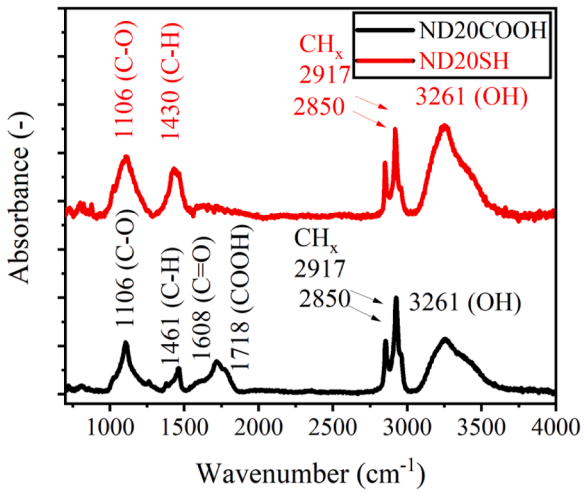

Fig. 3. FTIR spectra of ND20-COOH and ND20-SH samples. The spectra were vertically shifted for the sake of visibility.

be associated with C–N, C=N, and sp^2-related carbon vibrations [65].

Elemental analysis obtained from XPS (Table 2) confirmed a significant increase in both sulfur and nitrogen content after surface modification.

The C 1s spectrum of ND20-COOH (Fig. 4**a**) showed components corresponding to C–C/C–H, C–O, C=O, and O–C=O groups. After

Table 2
Elemental analysis of ND20-COOH and ND20-SH from XPS analysis. The values are in atomic concentrations (%).

	C	N	O	S
ND20-COOH	64.7	0.8	34.5	-
ND20-SH	56.2	3.8	37.1	3.0

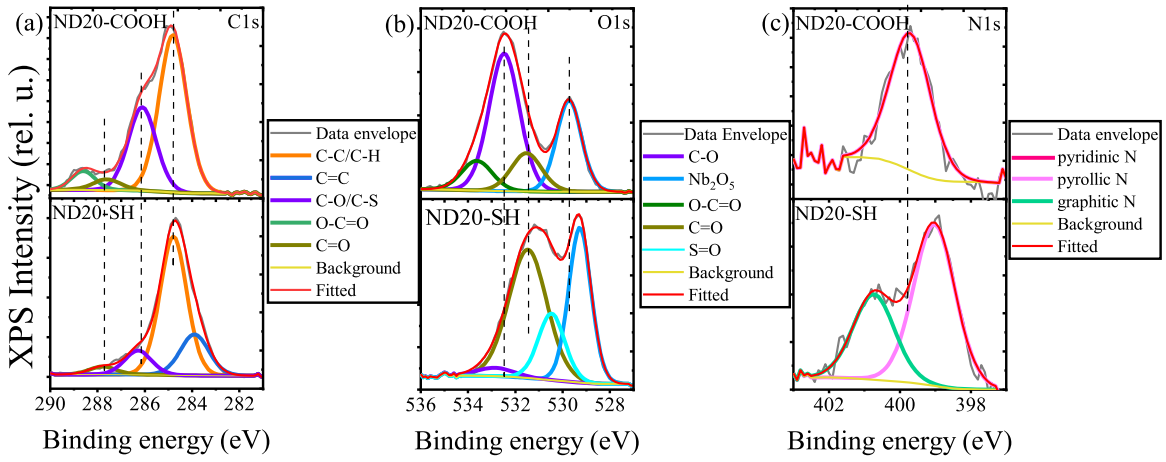

Fig. 4. **(a)** C 1s, **(b)** O 1s, **(c)** N 1s photoelectron spectra of ND20-COOH and ND20-SH samples.

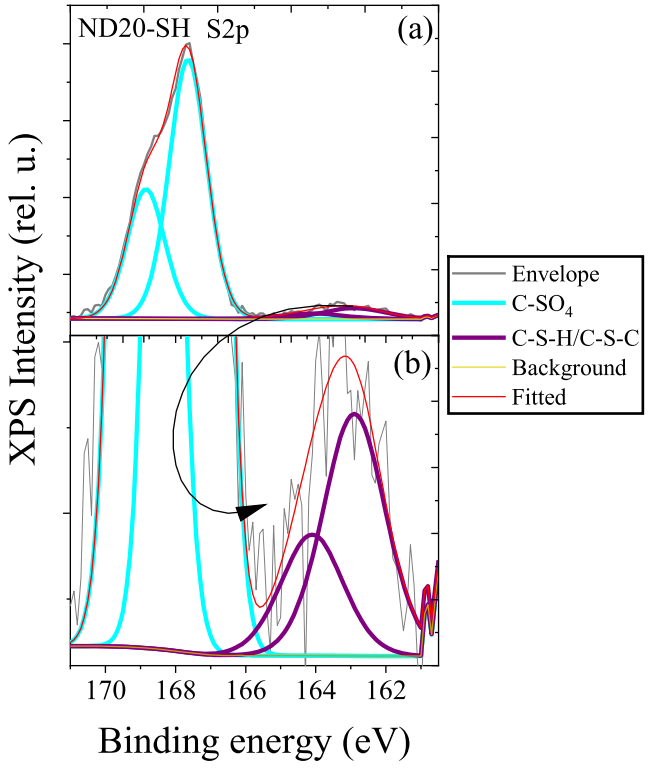

Fig. 5. S 2p photoelectron spectra of ND20SH sample. (a) Full spectrum and (b) zoom-in spectrum.

surface modification, the intensities of C–O, C=O, and COOH components decreased, consistent with FTIR results. Importantly, a new C=C peak emerged at ~283.9 eV, indicating the formation of sp^2-hybridized carbon.

The O 1s spectra (Fig. 4**b**) of ND20-COOH showed distinct C–O, C=O, and O–C=O components [66], alongside a substrate-related Nb_2O_5 peak at ~529 eV. In ND20-SH, the O–C=O component was largely absent, and a new contribution at ~530.6 eV was observed, assigned to S=O species [67,68].

The N 1s spectrum (Fig. 4**c**) of ND20-COOH showed a single component at ~399.6 eV, attributable to pyrrolic N–sp^3–C nitrogen. After modification, the ND20-SH sample exhibited two major components: a peak at ~399.0 eV corresponding to pyridinic or imide-like nitrogen, and a peak at ~400.7 eV attributed to graphitic/quaternary nitrogen [69]. These signatures are reported features of sp^2-bonded C–N aromatic domains, including triazine-like or carbon-nitride-like motifs [70–72], and are consistent with the formation of conjugated nitrogen-rich surface species during the thiourea reaction [73].

The S 2p spectrum of ND20-SH (Fig. 5) contained two chemically distinct sulfur contributions: a major component at ~167.6 eV corresponding to oxidized sulfur species ($S=O_x$), and a smaller peak at ~162.9 eV assigned to thiol or sulfide-like sulfur (C–S–H / C–S–C). The dominance of oxidized sulfur is expected, as thiol groups are prone to oxidation upon heating, air exposure, and X-ray irradiation. The presence of both reduced and oxidized sulfur confirms that thiourea-derived sulfur species are incorporated into the surface in multiple chemical environments.

We report the peak fitting parameters in Tables 3, 4, 5, and 6.

Raman spectra recorded under 785 nm excitation (Fig. 6**a**) showed the characteristic diamond peak at 1331 cm^{-1}, the trans-polyacetylene mode [74,75] at ~1427 cm^{-1}, and a weak sp^2 G band. The similarity between ND20-COOH and ND20-SH spectra under 785 nm excitation indicates that no extensive graphitic overlayer is formed. The calculated I_D/I_G peak ratios were 0.24 and 0.29 for ND20-COOH and ND20-SH, respectively, indicating some decrease in the graphitic surface groups after thiourea surface modification. We note that the reduced graphitic content generally improves the charge state stability of NV^- as graphitic surface groups typically act as hole sources under green illumination [76].

In contrast, Raman spectra obtained at 325 nm excitation (Fig. 6**b**) showed a pronounced increase in the G-band intensity for the ND20-SH sample. UV excitation is known to be highly sensitive to small sp^2

Table 3
Peak fitting parameters and component intensities of C1s photoelectron spectra of ND20-COOH and ND20-SH samples. B. E. means binding energy and I. r. means intensity ratio.

	O-C=O		C=O		C-O/C-S		C-C/C-H		C=C	
	B.E. (eV)	I. r. (%)	B.E. (eV)	I. r. (%)	B.E. (eV)	I. r. (%)	B.E. (eV)	I. r. (%)	B.E. (eV)	I. r. (%)
ND20-COOH	288.6	6	287.6	4	286.1	31.2	284.8	58.7	-	-
ND20-SH	-	-	287.8	3.7	286.3	11.2	284.8	64.7	283.9	20.4

Table 4
Peak fitting parameters and component intensities of O1s photoelectron spectra of ND20-COOH and ND20-SH samples. B. E. means binding energy and I. r. means intensity ratio.

	O-C=O		C-O		C=O		S=O		Nb_2O_5	
	B.E. (eV)	I. r. (%)	B.E. (eV)	I. r. (%)	B.E. (eV)	I. r. (%)	B.E. (eV)	I. r. (%)	B.E. (eV)	I. r. (%)
ND20-COOH	533.5	10.7	532.4	49.1	531.4	13.7	-	-	530.3	26.6
ND20-SH	-	-	532.9	3	531.5	46.9	530.6	16.9	530.2	33.2

Table 5
Peak fitting parameters and component intensities of N1s photoelectron spectra of ND20-COOH and ND20-SH samples. B. E. means binding energy and I. r. means intensity ratio.

	Pyridinic N		Pyrollic N		Graphitic N	
	B.E. (eV)	I. r. (%)	B.E. (eV)	I. r. (%)	B.E. (eV)	I. r. (%)
ND20-COOH	-	-	399.6	100	-	-
ND20-SH	399	61	-	-	400.7	39

clusters and conjugated C–N domains, thereby selectively enhancing Raman scattering from these species. The increased G-band intensity is consistent with the XPS-derived evidence of sp^2 carbon formation and nitrogen-rich conjugated fragments.

These spectral features indicate the formation of short, conjugated sp^2 segments attached to the diamond surface by sigma-bonds, which do not form extended graphitic layers but are sufficiently conjugated to be resonantly enhanced under UV excitation [77–80]. These results strongly indicate that the sp^2 carbon in the aromatic fragments does not produce low-energy acceptor levels, so it should have no negative impact on the charge state stability of NV^- under green illumination.

Indeed, given these differences in surface chemistry and colloidal behavior, an important question is how the modified surface affects the optical properties of the NV centers. Surface terminations can modulate the local electronic environment by pinning the Fermi level or altering the near-surface band bending, thereby influencing whether the NV defect retains or loses an electron. In practical terms, these effects determine the relative populations of the negatively charged NV^- and the neutral NV^0 states.

Table 6
Peak fitting parameters and component intensities of $S2p_{3/2}$ photoelectron spectra of ND20-COOH and ND20-SH samples. B. E. means binding energy and I. r. means intensity ratio.

	$C\text{-}SO_x$		C-SH	
	B.E. (eV)	I. r. (%)	B.E. (eV)	I. r. (%)
ND20-COOH	-	-	-	-
ND20-SH	167.6	93.5	162.9	6.5

To evaluate how the new surface functionalities influence the charge-state distribution, we recorded photoluminescence (PL) spectra of ensembles of NV centers before and after surface modification. The resulting spectra are presented in Fig. 7. The spectra represent the averages of at least seven individual measurements for each sample. The NV^- fractions extracted from the photoluminescence spectra of the ND–COOH and ND–SH samples, together with their corresponding statistical parameters, are summarized in Table 7. The relative increase in the NV^- fraction following surface modification, including the propagated uncertainties, is displayed in Fig. 8, while the inset highlights the mean NV^- fractions for the ND–COOH and ND–SH samples. The PL measurements were repeated after 1 month, 2 months and 1 year and no significant changes were observed during the time, indicating the long-term stability of NV^- centers.

The PL spectra displayed characteristic features of NV centers: the zero-phonon lines (ZPLs) of NV^0 and NV^- at 575 and 637 nm, respectively, and the vibrational bands of NV^- at 662 and 680 nm. As shown in Fig. 7 and Table 7, the NV^- fraction of ND-COOH samples generally increased with the nominal sizes. After the thiolation reaction, an increase in the NV^- fraction was observed, specifically notable for the 20 nm sample, which reaches the values comparable to those of the 140 nm sample. Although thiol groups are frequently described as soft nucleophiles with electron-donating tendencies, the surface chemistry produced in this reaction is more complex than the formation of isolated –SH groups. FTIR, XPS, and UV–excited Raman measurements indicated the presence of additional sp^2-hybridized carbon–nitrogen species, short conjugated C–N fragments formed under the applied reaction

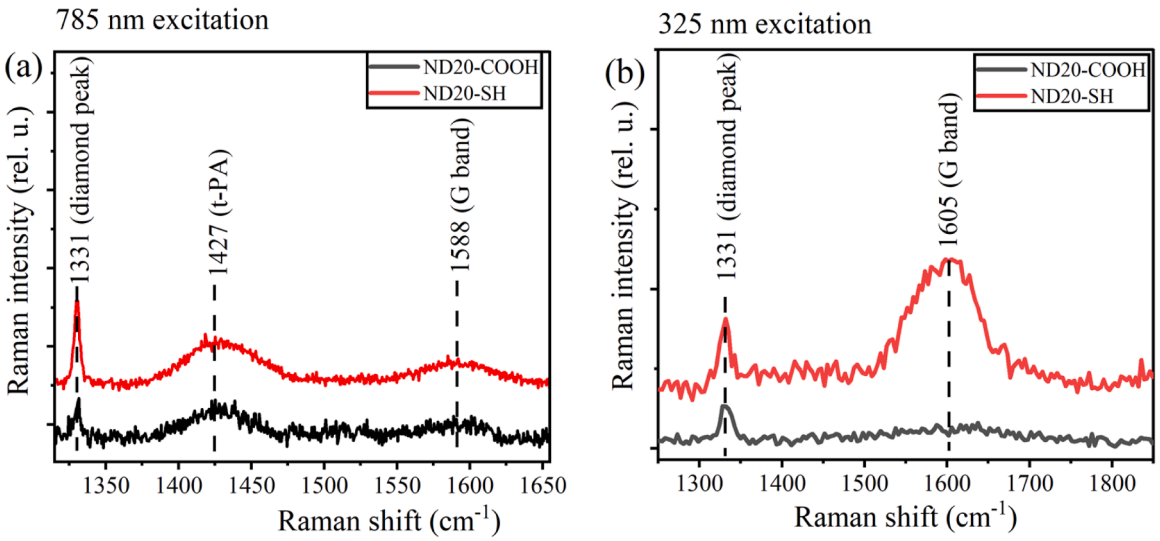

Fig. 6. Raman spectra of ND20-COOH and ND20-SH samples upon (a) 325 nm (b) 785 nm excitation.

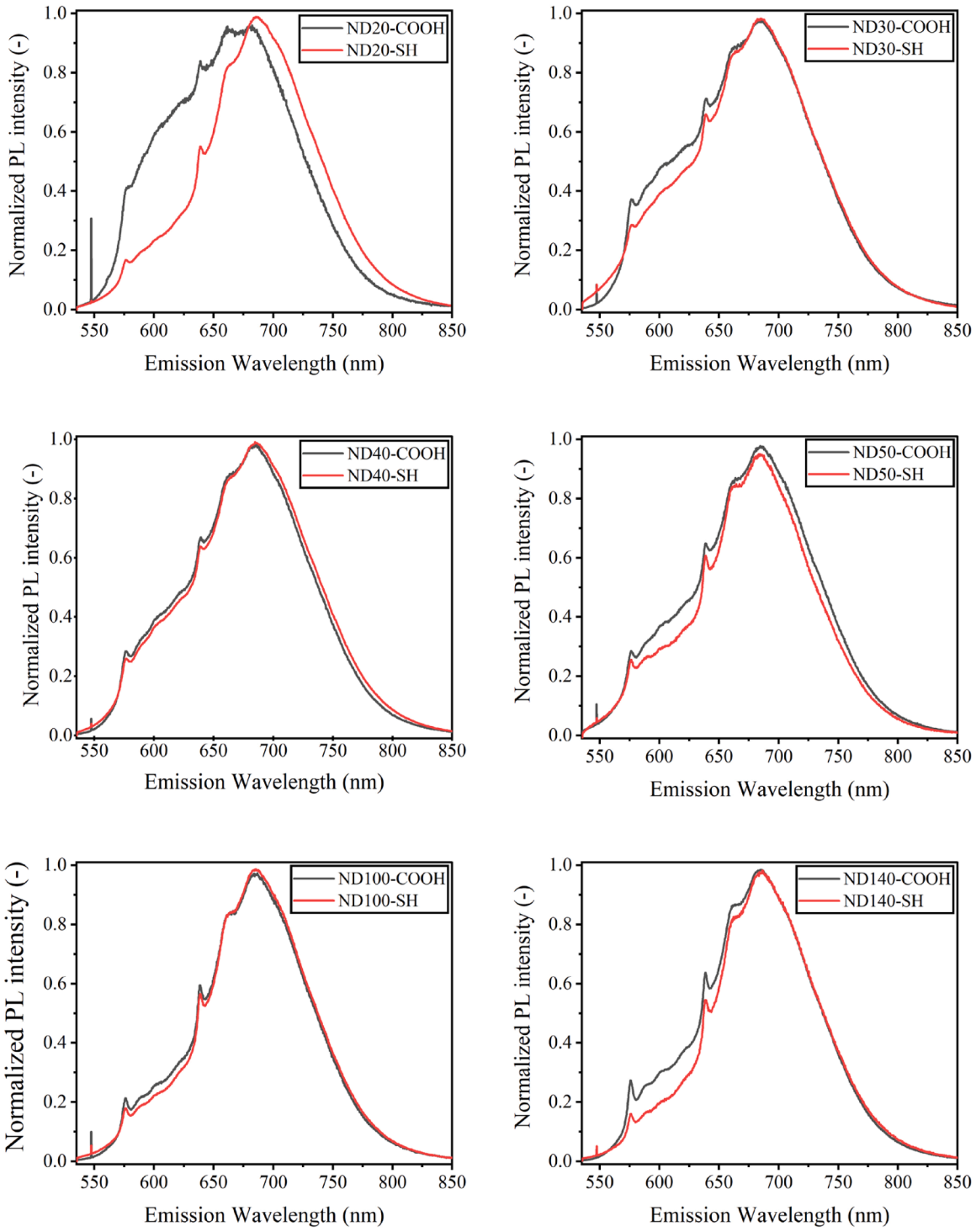

Fig. 7. PL spectra of ND-COOH and ND-SH samples upon 532 nm excitation and P = 36 μW. The spectra shown represent the average of at least 7 individual measurements. The sharp peak observed at 545 nm is the first-order Raman peak of the silicon substrate.

conditions. Such fragments are consistent with partially condensed triazine- or carbon-nitride-like motifs, which are known to act as electron-rich surface domains.

These nitrogen-containing sp^2 units can interact electronically with the diamond surface and act as local electron reservoirs, thereby raising the surface Fermi level and stabilizing the negatively charged NV^- state. Even when connected through S–C linkages, such domains can remain sufficiently coupled to the surface to influence charge transfer. In this context, the observed enhancement of the NV^- fraction is therefore best explained by the combined effect of surface thiol and oxygen-related groups, and nitrogen-rich conjugated byproducts, which together introduce electron-donating and n-type surface character. This shifts the NV^0/NV^- equilibrium toward NV^-, particularly in small nanodiamonds, where surface charge compensation is most crucial.

4. Conclusions

In this work, we modified carboxyl-terminated FNDs using a

Table 7
NV^- fraction of ND-COOH and ND-SH samples and their statistical parameters under 532 nm excitation.

Size (nm)	COOH Mean (SD)	SH Mean (SD)	Enhancement (%)
20	46 (1.5)	80 (2.3)	72
30	59 (4.3)	67 (5.3)	13
40	65 (2.0)	69 (3.3)	5
50	67 (3.5)	73 (9.4)	9
100	76 (5.7)	79 (4.8)	4
140	72 (7.7)	81 (5.6)	12

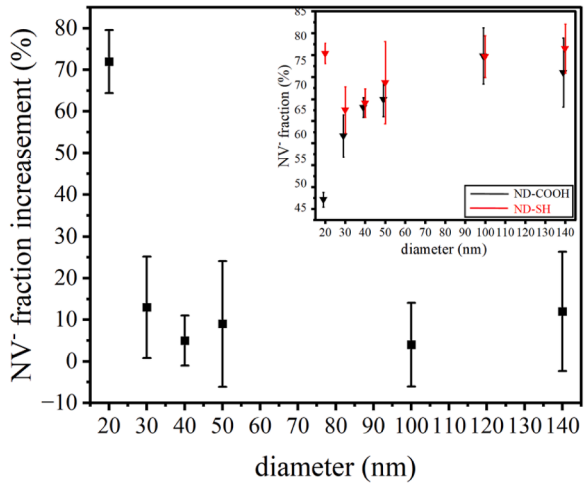

Fig. 8. NV^- fraction enhancement during the surface modification including propagated error values under 532 nm excitation at 36 μW. The inset shows mean values, and the error bars represent standard deviations. For clarity, the mean values and error bars of the ND–SH samples are slightly shifted horizontally.

thiourea-based reaction. FTIR, XPS, and Raman measurements showed that, in addition to thiol formation, the reaction generated oxidized sulfur species and nitrogen-containing sp^2 domains. These new surface functionalities altered the charge environment and colloidal behavior of the particles, resulting in a more than 70% increase in the NV^- population for the smallest, 20 nm nanodiamonds, as revealed by photoluminescence measurements. More on that, the existing thiol groups at the surface provide chemically versatile and biologically relevant surface functionality, enabling robust conjugation to biomolecules, polymers, and inorganic interfaces. For nanoscale thermometry and magnetic field sensing, thiourea-modified nanodiamonds offer improved surface passivation and reduced charge-state fluctuations, which might enable higher temperature sensitivity and greater measurement reliability at the subcellular or interfacial scale [81], and are essential for preserving ODMR contrast [82] and spin coherence in complex biological or chemical environments.

Data availability statement

All data available from the authors open reasonable requests.

Funding

This study was supported by the Quantum Information National Laboratory sponsored by National Research, Development and Innovation Fund of Hungary (NKFIH) Grant No. 2022-2.1.1-NL-2022-00004 for the XPS investigations. The materials preparation was supported by the Ministry of Culture and Innovation of Hungary from NKFIH, financed under the TKP2021-NVA funding scheme (Project no. TKP2021-NVA-04). S. L. was supported by the Bolyai János Research Scholarship of the Hungarian Academy of Sciences.

CRediT authorship contribution statement

Péter Rózsa: Writing – review & editing, Writing – original draft, Methodology, Investigation, Formal analysis, Data curation. **Olga Krafcsik:** Methodology, Investigation, Formal analysis, Data curation. **Sándor Lenk:** Methodology, Investigation. **David Beke:** Writing – review & editing, Validation, Methodology, Formal analysis, Conceptualization. **Adam Gali:** Writing – review & editing, Writing – original draft, Validation, Supervision, Resources, Project administration, Funding acquisition, Conceptualization.

Declaration of competing interest

The authors declare that they have no known competing financial interests or personal relationships that could have appeared to influence the work reported in this paper.

Acknowledgments

We acknowledge the discussion with Miklós Veres. The research reported in this paper and carried out at HUN-REN Wigner Research Centre for Physics is supported by the infrastructure of the Hungarian Academy of Sciences.

References

[1] C.Y. Fang, V. Vaijayanthimala, C.A. Cheng, S.H. Yeh, C.F. Chang, C.L. Li, H. C. Chang, The exocytosis of fluorescent nanodiamond and its use as a long-term cell tracker, Small. 7 (23) (2011) 3363–3370, https://doi.org/10.1002/smll.201101233.
[2] V. Vaijayanthimala, P.Y. Cheng, S.H. Yeh, K.K. Liu, C.H. Hsiao, J.I. Chao, H. C. Chang, The long-term stability and biocompatibility of fluorescent nanodiamond as an in vivo contrast agent, Biomaterials 33 (31) (2012) 7794–7802, https://doi.org/10.1016/j.biomaterials.2012.06.084.
[3] S.J. Yu, M.W. Kang, H.C. Chang, K.M. Chen, Y.C. Yu, Bright fluorescent nanodiamonds: No photobleaching and low cytotoxicity, J. Am. Chem. Soc. 127 (50) (2005) 17604–17605, https://doi.org/10.1021/ja0567081.
[4] F.A. Pedroza-Montero, J.N. Pedroza-Montero, O. Álvarez-Bajo, E. Silva-Campa, D. Soto-Puebla, M. Barboza-Flores, Study of fluorescent nanodiamonds concentrations in aqueous solutions for biological applications, Opt. Mater. (Amst) 140 (2023) 113872, https://doi.org/10.1016/j.optmat.2023.113872.
[5] L.A. Stewart, Y. Zhai, J.M. Dawes, M.J. Steel, J.R. Rabeau, M.J. Withford, Single photon emission from diamond nanocrystals in an opal photonic crystal, Opt. Express, OE 17 (20) (2009) 18044–18053, https://doi.org/10.1364/OE.17.018044.
[6] M. Tsukamoto, S. Ito, K. Ogawa, Y. Ashida, K. Sasaki, K. Kobayashi, Accurate magnetic field imaging using nanodiamond quantum sensors enhanced by machine learning, Sci. Rep. 12 (1) (2022) 13942, https://doi.org/10.1038/s41598-022-18115-w.
[7] M. Jani, P. Czarnecka, Z. Orzechowska, M. Mrózek, W. Gawlik, A. M. Wojciechowski, Sensing of magnetic-field gradients with nanodiamonds on optical glass-fiber facets, ACS. Appl. Nano Mater. 6 (13) (2023) 11077–11084, https://doi.org/10.1021/acsanm.3c00887.
[8] F. Dolde, H. Fedder, M.W. Doherty, T. Nöbauer, F. Rempp, G. Balasubramanian, T. Wolf, F. Reinhard, L.C.L. Hollenberg, F. Jelezko, J. Wrachtrup, Electric-field sensing using single diamond spins, Nat. Phys. 7 (6) (2011) 459–463, https://doi.org/10.1038/nphys1969.
[9] J.R. Maze, A. Gali, E. Togan, Y. Chu, A. Trifonov, E. Kaxiras, M.D. Lukin, Properties of nitrogen-vacancy centers in diamond: the group theoretic approach, New. J. Phys. 13 (2) (2011) 025025, https://doi.org/10.1088/1367-2630/13/2/025025.
[10] F.A. Pedroza-Montero, K.J. Santacruz-Gomez, R. Meléndrez-Amavizca, M. Barboza-Flores, Commercial nanodiamonds for precise fluorescence-based temperature sensing, Appl. Phys. Lett. 125 (7) (2024) 073701, https://doi.org/10.1063/5.0219532.
[11] T. Sekiguchi, S. Sotoma, Y. Harada, Fluorescent nanodiamonds as a robust temperature sensor inside a single cell, Biophys. Physicobiol. 15 (2018) 229–234, https://doi.org/10.2142/biophysico.15.0_229.
[12] G. Kucsko, P.C. Maurer, N.Y. Yao, M. Kubo, H.J. Noh, P.K. Lo, H. Park, M.D. Lukin, Nanometre-scale thermometry in a living cell, Nature 500 (7460) (2013) 54–58, https://doi.org/10.1038/nature12373.
[13] M.H. Alkahtani, F. Alghannam, L. Jiang, A.A. Rampersaud, R. Brick, C.L. Gomes, M.O. Scully, P.R. Hemmer, Fluorescent nanodiamonds for luminescent thermometry in the biological transparency window, Opt. Lett., OL 43 (14) (2018) 3317–3320, https://doi.org/10.1364/OL.43.003317.

[14] T.H.H. Le, R. Hsin, D.T. Vo, Y.K. Tzeng, T.N. Le, W.W. Hsiao, Nanoscale thermometry with fluorescent nanodiamonds. Nanodiamonds in Analytical and Biological Sciences, John Wiley & Sons, Ltd, 2023, pp. 156–170, https://doi.org/10.1002/9781394202164.ch9.
[15] A. Sigaeva, A. Hochstetter, S. Bouyim, M. Chipaux, M. Stejfova, P. Cigler, R. Schirhagl, Single-particle tracking and trajectory analysis of fluorescent nanodiamonds in cell-free environment and live cells, Small. 18 (39) (2022) 2201395, https://doi.org/10.1002/smll.202201395.
[16] R. Li, T.A. Vedelaar, A. Sigaeva, Y. Zhang, K. Wu, H. Wang, X. Wu, P. Olinga, M. K. Wlodarzyk-Biegun, R. Schirhagl, Fluorescent nanodiamonds for tracking single polymer particles in cells and tissues, Anal. Chem. 95 (35) (2023) 13046–13054, https://doi.org/10.1021/acs.analchem.3c01452.
[17] W.W.W. Hsiao, Y.Y. Hui, P.C. Tsai, H.C. Chang, Fluorescent nanodiamond: a versatile tool for long-term cell tracking, super-resolution imaging, and nanoscale temperature sensing, Acc. Chem. Res. 49 (3) (2016) 400–407, https://doi.org/10.1021/acs.accounts.5b00484.
[18] C. Fryer, P. Murray, H. Zhang, Modification of nanodiamonds for fluorescence bioimaging, RSC. Adv. 14 (7) (2024) 4633–4644, https://doi.org/10.1039/D3RA08762J.
[19] Y.C. Wu, Y.C. Wang, W.T. Wang, H.M.D. Wang, H.H. Lin, L.J. Su, Y.R. Kuo, C.S. Lai, M.L. Ho, J. Yu, Fluorescent nanodiamonds enable long-term detection of human adipose-derived stem/stromal cells in an In vivo chondrogenesis model using decellularized extracellular matrices and fibrin glue polymer, Polymers. (Basel) 11 (9) (2019) 1391, https://doi.org/10.3390/polym11091391.
[20] M.W. Doherty, N.B. Manson, P. Delaney, F. Jelezko, J. Wrachtrup, L.C. L. Hollenberg, The nitrogen-vacancy colour centre in diamond, Phys. Rep. 528 (1) (2013) 1–45, https://doi.org/10.1016/j.physrep.2013.02.001.
[21] J.N. Neethirajan, T. Hache, D. Paone, D. Pinto, A. Denisenko, R. Stöhr, P. Udvarhelyi, A. Pershin, A. Gali, J. Wrachtrup, K. Kern, A. Singha, Controlled surface modification to revive shallow NV– centers, Nano Lett 23 (7) (2023) 2563–2569, https://doi.org/10.1021/acs.nanolett.2c04733.
[22] S. Karaveli, O. Gaathon, A. Wolcott, R. Sakakibara, O.A. Shemesh, D.S. Peterka, E. S. Boyden, J.S. Owen, R. Yuste, D. Englund, Modulation of nitrogen vacancy charge state and fluorescence in nanodiamonds using electrochemical potential, Proceedings of the National Academy of Sciences 113 (15) (2016) 3938–3943, https://doi.org/10.1073/pnas.1504451113.
[23] A. Krueger, D. Lang, Functionality Is Key: Recent Progress in the Surface Modification of Nanodiamond, Advanced Functional Materials 22 (5) (2012) 890–906, https://doi.org/10.1002/adfm.201102670.
[24] E. Janitz, K. Herb, L.A. Völker, W.S. Huxter, C.L. Degen, J.M. Abendroth, Diamond surface engineering for molecular sensing with nitrogen—vacancy centers, J. Mater. Chem. C 10 (37) (2022) 13533–13569, https://doi.org/10.1039/D2TC01258H.
[25] A. Nagl, S.R. Hemelaar, R. Schirhagl, Improving surface and defect center chemistry of fluorescent nanodiamonds for imaging purposes—a review, Anal. Bioanal. Chem. 407 (25) (2015) 7521–7536, https://doi.org/10.1007/s00216-015-8849-1.
[26] G. Reina, L. Zhao, A. Bianco, N. Komatsu, Chemical functionalization of nanodiamonds: opportunities and challenges ahead, Angewandte Chemie. Int. Edit. 58 (50) (2019) 17918–17929, https://doi.org/10.1002/anie.201905997.
[27] H. Yamano, S. Kawai, K. Kato, T. Kageura, M. Inaba, T. Okada, I. Higashimata, M. Haruyama, T. Tanii, K. Yamada, S. Onoda, W. Kada, O. Hanaizumi, T. Teraji, J. Isoya, H. Kawarada, Charge State stabilization of shallow nitrogen vacancy centers in diamond by oxygen surface modification, JPN. J. Appl. Phys. 56 (4S) (2017) 04CK08, https://doi.org/10.7567/JJAP.56.04CK08.
[28] M.V. Hauf, B. Grotz, B. Naydenov, M. Dankerl, S. Pezzagna, J. Meijer, F. Jelezko, J. Wrachtrup, M. Stutzmann, F. Reinhard, J.A. Garrido, Chemical control of the charge State of nitrogen-vacancy centers in diamond, Phys. Rev. B 83 (8) (2011) 081304, https://doi.org/10.1103/PhysRevB.83.081304.
[29] F. Fávaro de Oliveira, S.A. Momenzadeh, Y. Wang, M. Konuma, M. Markham, A. M. Edmonds, A. Denisenko, J. Wrachtrup, Effect of low-damage inductively coupled plasma on shallow nitrogen-vacancy centers in diamond, Appl. Phys. Lett. 107 (7) (2015) 073107, https://doi.org/10.1063/1.4929356.
[30] M. Kim, H.J. Mamin, M.H. Sherwood, C.T. Rettner, J. Frommer, D. Rugar, Effect of oxygen plasma and thermal oxidation on shallow nitrogen-vacancy centers in diamond, Appl. Phys. Lett. 105 (4) (2014) 042406, https://doi.org/10.1063/1.4891839.
[31] M. Kaviani, P. Deák, B. Aradi, T. Frauenheim, J.P. Chou, A. Gali, Proper surface termination for luminescent near-surface NV centers in diamond, Nano Lett. 14 (8) (2014) 4772–4777, https://doi.org/10.1021/nl501927y.
[32] T. Kageura, K. Kato, H. Yamano, E. Suaebah, M. Kajiya, S. Kawai, M. Inaba, T. Tanii, M. Haruyama, K. Yamada, S. Onoda, W. Kada, O. Hanaizumi, T. Teraji, J. Isoya, S. Kono, H. Kawarada, Effect of a radical exposure nitridation surface on the charge stability of shallow nitrogen-vacancy centers in diamond, Appl. Phys. Express. 10 (5) (2017) 055503, https://doi.org/10.7567/APEX.10.055503.
[33] J.P. Chou, A. Retzker, A. Gali, Nitrogen-terminated diamond (111) surface for room-temperature quantum sensing and simulation, Nano Lett. 17 (4) (2017) 2294–2298, https://doi.org/10.1021/acs.nanolett.6b05023.
[34] S. Kawai, H. Yamano, T. Sonoda, K. Kato, J.J. Buendia, T. Kageura, R. Fukuda, T. Okada, T. Tanii, T. Higuchi, M. Haruyama, K. Yamada, S. Onoda, T. Ohshima, W. Kada, O. Hanaizumi, A. Stacey, T. Teraji, S. Kono, J. Isoya, H. Kawarada, Nitrogen-terminated diamond surface for nanoscale NMR by shallow Nitrogen-vacancy centers, J. Phys. Chem. C 123 (6) (2019) 3594–3604, https://doi.org/10.1021/acs.jpcc.8b11274.
[35] K.J. Rietwyk, S.L. Wong, L. Cao, K.M. O'Donnell, L. Ley, A.T.S. Wee, C.I. Pakes, Work function and electron affinity of the fluorine-terminated (100) diamond surface, Appl. Phys. Lett. 102 (9) (2013) 091604, https://doi.org/10.1063/1.4793999.
[36] L.V.H. Rodgers, S.T. Nguyen, J.H. Cox, K. Zervas, Z. Yuan, S. Sangtawesin, A. Stacey, C. Jaye, C. Weiland, A. Pershin, A. Gali, L. Thomsen, S.A. Meynell, L. B. Hughes, A.C.B. Jayich, X. Gui, R.J. Cava, R.R. Knowles, N.P. de Leon, Diamond surface functionalization via visible light–Driven C–H activation for nanoscale quantum sensing, Proceed. Nat. Acad. Sci. 121 (11) (2024) e2316032121, https://doi.org/10.1073/pnas.2316032121.
[37] M.V. Hauf, B. Grotz, B. Naydenov, M. Dankerl, S. Pezzagna, J. Meijer, F. Jelezko, J. Wrachtrup, M. Stutzmann, F. Reinhard, J.A. Garrido, Chemical control of the charge State of nitrogen-vacancy centers in diamond, Phys. Rev. B 83 (8) (2011) 081304, https://doi.org/10.1103/PhysRevB.83.081304.
[38] S.Y. Choh, D. Cross, C. Wang, Facile synthesis and characterization of disulfide-cross-linked hyaluronic acid hydrogels for protein delivery and cell encapsulation, Biomacromolecules. 12 (4) (2011) 1126–1136, https://doi.org/10.1021/bm101451k.
[39] A.B. Lowe, Thiol-ene "click" reactions and recent applications in polymer and materials synthesis, Polym. Chem. 1 (1) (2010) 17–36, https://doi.org/10.1039/B9PY00216B.
[40] C. Vericat, M.E. Vela, G. Benitez, P. Carro, R.C. Salvarezza, Self-assembled monolayers of thiols and dithiols on gold: new challenges for a well-known system, Chem. Soc. Rev. 39 (5) (2010) 1805–1834, https://doi.org/10.1039/B907301A.
[41] G. Li, Z. Zhao, J. Liu, G. Jiang, Effective heavy metal removal from aqueous systems by thiol functionalized magnetic mesoporous silica, J. Hazard. Mater. 192 (1) (2011) 277–283, https://doi.org/10.1016/j.jhazmat.2011.05.015.
[42] S. Xu, X. Han, A novel method to construct a third-generation biosensor: self-assembling gold nanoparticles on thiol-functionalized poly(Styrene-Co-Acrylic Acid) nanospheres, Biosens. Bioelectron. 19 (9) (2004) 1117–1120, https://doi.org/10.1016/j.bios.2003.09.007.
[43] T. Potta, C. Chun, S.-C. Song, Chemically crosslinkable thermosensitive polyphosphazene gels as injectable materials for biomedical applications, Biomaterials 30 (31) (2009) 6178–6192, https://doi.org/10.1016/j.biomaterials.2009.08.015.
[44] S. Zhang, G. Leem, L. Srisombat, T.R. Lee, Rationally designed ligands that inhibit the aggregation of large gold nanoparticles in solution, J. Am. Chem. Soc. 130 (1) (2008) 113–120, https://doi.org/10.1021/ja0724588.
[45] E. Janitz, K. Herb, L. A. Völker, W. S. Huxter, C. L. Degen, J. M. Abendroth, Diamond surface engineering for molecular sensing with nitrogen—vacancy centers, J. Mater. Chem. C 10 (37) (2022) 13533–13569, https://doi.org/10.1039/D2TC01258H.
[46] T. Fujisaku, R. Tanabe, S. Onoda, R. Kubota, T.F. Segawa, F.T.K. So, T. Ohshima, I. Hamachi, M. Shirakawa, R. Igarashi, pH nanosensor using electronic spins in diamond, ACS. Nano 13 (10) (2019) 11726–11732, https://doi.org/10.1021/acsnano.9b05342.
[47] A. Kundu, F. Martinelli, G. Galli, Designing optically addressable nitrogen-vacancy centers in ultrasmall nanodiamonds: insights from first-principles calculations, J. Phys. Chem. Lett. 16 (8) (2025) 1973–1979, https://doi.org/10.1021/acs.jpclett.5c00355.
[48] Y. Wu, T. Weil, Recent developments of nanodiamond quantum sensors for biological applications, Adv. Sci. 9 (19) (2022) 2200059, https://doi.org/10.1002/advs.202200059.
[49] T. Fujisaku, R. Tanabe, S. Onoda, R. Kubota, T.F. Segawa, F.T.K. So, T. Ohshima, I. Hamachi, M. Shirakawa, R. Igarashi, pH nanosensor using electronic spins in diamond, ACS. Nano 13 (10) (2019) 11726–11732, https://doi.org/10.1021/acsnano.9b05342.
[50] B.A. Tkachenko, N.A. Fokina, L.V. Chernish, J.E.P. Dahl, S. Liu, R.M.K. Carlson, A. A. Fokin, P.R. Schreiner, Functionalized nanodiamonds part 3: thiolation of tertiary/bridgehead alcohols, Org. Lett. 8 (9) (2006) 1767–1770, https://doi.org/10.1021/ol053136g.
[51] M.H. Hsu, H. Chuang, F.Y. Cheng, Y.P. Huang, C.C. Han, J.Y. Chen, S.C. Huang, J. K. Chen, D.S. Wu, H.L. Chu, C.C. Chang, Directly thiolated modification onto the surface of detonation nanodiamonds, ACS. Appl. Mater. Interfaces. 6 (10) (2014) 7198–7203, https://doi.org/10.1021/am500324z.
[52] D.M. Parker, A.J. Lineweaver, A.D. Quast, I. Zharov, J.S. Shumaker-Parry, Thiol-terminated nanodiamond powders for support of gold nanoparticle catalysts, Diam. Relat. Mater. 116 (2021) 108449, https://doi.org/10.1016/j.diamond.2021.108449.
[53] S. Kawai, H. Yamano, T. Sonoda, K. Kato, J.J. Buendia, T. Kageura, R. Fukuda, T. Okada, T. Tanii, T. Higuchi, M. Haruyama, K. Yamada, S. Onoda, T. Ohshima, W. Kada, O. Hanaizumi, A. Stacey, T. Teraji, S. Kono, J. Isoya, H. Kawarada, Nitrogen-terminated diamond surface for nanoscale NMR by shallow Nitrogen-vacancy centers, J. Phys. Chem. C 123 (6) (2019) 3594–3604, https://doi.org/10.1021/acs.jpcc.8b11274.
[54] J.M. Abendroth, K. Herb, E. Janitz, T. Zhu, L.A. Völker, C.L. Degen, Single-nitrogen–Vacancy NMR of amine-functionalized diamond surfaces, Nano Lett. 22 (18) (2022) 7294–7303, https://doi.org/10.1021/acs.nanolett.2c00533.
[55] M. Haruyama, Y. Okigawa, M. Okada, H. Nakajima, T. Okazaki, H. Kato, T. Makino, T. Yamada, Charge stabilization of shallow nitrogen-vacancy centers using graphene/diamond junctions, Appl. Phys. Lett. 122 (14) (2023) 141601, https://doi.org/10.1063/5.0143062.
[56] W.K. Lo, Y. Zhang, H.Y. Chow, J. Wu, M.Y. Leung, K.O. Ho, X. Du, Y. Chen, Y. Shen, D. Pan, S. Yang, Enhancement of quantum coherence in solid-State qubits via interface engineering, Nat. Commun. 16 (1) (2025) 5984, https://doi.org/10.1038/s41467-025-61026-3.
[57] Y. Hao, Z. Yang, Z. Li, X. Kong, W. Tang, T. Xie, S. Xu, X. Ye, P. Yu, P. Wang, Y. Wang, Z. Qiao, L. Gao, J.H. Jiang, F. Shi, J. Du, Coherence enhancement via a

diamond-graphene hybrid for nanoscale quantum sensing, Natl. Sci. Rev. 12 (5) (2025) nwaf076, https://doi.org/10.1093/nsr/nwaf076.
[58] S.V. Makarov, A.K. Horváth, R. Silaghi-Dumitrescu, Q. Gao, Recent developments in the chemistry of thiourea oxides, Chem. – A European J. 20 (44) (2014) 14164–14176, https://doi.org/10.1002/chem.201403453.
[59] S. Sahu, P. Rani Sahoo, S. Patel, B.K. Mishra, Oxidation of thiourea and substituted thioureas: a review, J. Sulfur Chem. 32 (2) (2011) 171–197, https://doi.org/10.1080/17415993.2010.550294.
[60] G. Thalassinos, D.J. McCloskey, A. Mameli, A.J. Healey, C. Pattinson, D. Simpson, B.C. Gibson, A. Stacey, N. Dontschuk, P. Reineck, Robust quantification of the diamond nitrogen-vacancy center charge State via photoluminescence spectroscopy, APL. Photonics. 10 (10) (2025) 101102, https://doi.org/10.1063/5.0284237.
[61] S.T. Alsid, J.F. Barry, L.M. Pham, J.M. Schloss, M.F. O'Keeffe, P. Cappellaro, D. A. Braje, Photoluminescence decomposition analysis: a technique to characterize N - V creation in diamond, Phys. Rev. Applied 12 (4) (2019) 044003, https://doi.org/10.1103/PhysRevApplied.12.044003.
[62] S.A. Savinov, V.V. Sychev, D. Bi, Diamond nitrogen-vacancy center charge State ratio determination at a given sample point, J. Lumin. 248 (2022) 118981, https://doi.org/10.1016/j.jlumin.2022.118981.
[63] S. Sharma, Y. Walia, G. Grover, V. Sanjeev, Effect of surface modification of silica nanoparticles with thiol group on the shear thickening behaviors of the suspensions of silica nanoparticles in polyethylene glycol (PEG), IOP Conference Series: Mater. Sci. Eng. 1225 (2022) 012053, https://doi.org/10.1088/1757-899X/1225/1/012053.
[64] C.J. Huang, L.C. Wang, C.Y. Liu, A. Chiang, Y.C. Chang, Natural zwitterionic organosulfurs as surface ligands for antifouling and responsive properties, Biointerphases. 9 (2014) 029010, https://doi.org/10.1116/1.4869300.
[65] T. Petit, L. Puskar, FTIR spectroscopy of nanodiamonds: methods and interpretation, Diam. Relat. Mater. 89 (2018) 52–66, https://doi.org/10.1016/j.diamond.2018.08.005.
[66] N.-F. Chiu, M.-J. Tai, D. Nurrohman, T.-L. Lin, Y.-H. Wang, C.-Y. Chen, Immunoassay-Amplified Responses Using a Functionalized MoS2-Based SPR Biosensor to Detect PAPP-A2 in Maternal Serum Samples to Screen for Fetal Down's Syndrome, International Journal of Nanomedicine 16 (2021) 2715–2733. https://doi.org/10.2147/IJN.S296406.
[67] I. Herrmann, U.I. Kramm, J. Radnik, S. Fiechter, P. Bogdanoff, Influence of sulfur on the pyrolysis of CoTMPP as electrocatalyst for the oxygen reduction reaction, J. Electrochem. Soc. 156 (10) (2009) B1283, https://doi.org/10.1149/1.3185852.
[68] R.V. Siriwardane, Effect of O2 on the interaction of SO2 with CaO(100), iron deposited on CaO(100), and sodium deposited on CaO(100), J. Colloid. Interface Sci. 116 (2) (1987) 463–472, https://doi.org/10.1016/0021-9797(87)90142-1.
[69] I. Gouzman, R. Brener, A. Hoffman, Nitridation of diamond and graphite surfaces by low energy N+2 ion irradiation, Surf. Sci. 331–333 (1995) 283–288, https://doi.org/10.1016/0039-6028(95)00187-5.
[70] S. Yang, Z. Chen, L. Zou, R. Cao, Construction of thiadiazole-linked covalent organic frameworks via facile linkage conversion with superior photocatalytic properties, Adv. Sci. 10 (31) (2023) 2304697, https://doi.org/10.1002/advs.202304697.
[71] H. Tang, J. Sun, X. Yan, P. Wu, Electrochemical and adsorption behaviors of thiadiazole derivatives on the aluminum surface, RSC. Adv. 9 (59) (2019) 34617–34626, https://doi.org/10.1039/C9RA05740D.
[72] A.G. Ibrahim, A. Fouda, W. Elgammal, A. Eid, M. Elsenety, A. Emad, S. Hassan, New thiadiazole modified chitosan derivative to control the growth of Human pathogenic microbes and cancer cell lines, Sci. Rep. 12 (2022) 21423, https://doi.org/10.1038/s41598-022-25772-4.
[73] M.M.T. Khan, S. Srivastava, Some new ruthenium(III) schiff base complexes: a photoelectron spectroscopic study, Polyhedron 7 (12) (1988) 1063–1065, https://doi.org/10.1016/S0277-5387(00)86396-2.
[74] E. Cannuccia, Effect of the quantum zero-point atomic motion on the optical and electronic properties of diamond and trans-polyacetylene, Phys. Rev. Lett. 107 (25) (2011), https://doi.org/10.1103/PhysRevLett.107.255501.
[75] R. Pfeiffer, H. Kuzmany, P. Knoll, S. Bokova, N. Salk, B. Günther, Evidence for trans-polyacetylene in nano-crystalline diamond films, Diam. Relat. Mater. 12 (3) (2003) 268–271, https://doi.org/10.1016/S0925-9635(02)00336-9.
[76] A. Stacey, N. Dontschuk, J.P. Chou, D.A. Broadway, A.K. Schenk, M.J. Sear, J. P. Tetienne, A. Hoffman, S. Prawer, C.I. Pakes, A. Tadich, N.P. de Leon, A. Gali, L.C. L. Hollenberg, Evidence for primal Sp2 defects at the diamond surface: candidates for electron trapping and noise sources, Adv. Mater. Interfaces. 6 (3) (2019) 1801449, https://doi.org/10.1002/admi.201801449.
[77] A.C. Ferrari, Determination of bonding in diamond-like carbon by raman spectroscopy, Diam. Relat. Mater. 11 (3) (2002) 1053–1061, https://doi.org/10.1016/S0925-9635(01)00730-0.
[78] A.C. Ferrari, J. Robertson, A.C. Ferrari, J.Raman Robertson, Spectroscopy of amorphous, nanostructured, diamond–like carbon, and nanodiamond, Philosophi. Trans. Royal Soc. London. Series A 362 (1824) (2004) 2477–2512, https://doi.org/10.1098/rsta.2004.1452.
[79] J. Robertson, Diamond-like amorphous carbon, Mater. Sci. Eng. 37 (4) (2002) 129–281, https://doi.org/10.1016/S0927-796X(02)00005-0.
[80] M. Veres, S. Tóth, M. Koós, Grain Boundary Fine Structure of Ultrananocrystalline Diamond Thin Films Measured by Raman Scattering, Appl. Phys. Lett. 91 (3) (2007) 031913. https://doi.org/10.1063/1.2757122.
[81] T.N. Le, Y.T. Chiang, Y. Hui, T.H.H. Le, Y.K. Tzeng, N. Sharma, W.H. Chiang, W. W. Hsiao. vitro bioimaging of fluorescent nanodiamonds, Nanodiamonds in Analytical and Biological Sciences, John Wiley & Sons, Ltd, 2023, pp. 95–127, https://doi.org/10.1002/9781394202164.ch6.
[82] D.A. Simpson, A.J. Thompson, M. Kowarsky, N.F. Zeeshan, M.S.J. Barson, L.T. Hall, Y. Yan, S. Kaufmann, B.C. Johnson, T. Ohshima, F. Caruso, R.E. Scholten, R. B. Saint, M.J. Murray, L.C.L. Hollenberg, In Vivo Imaging and Tracking of Individual Nanodiamonds in Drosophila Melanogaster Embryos, Biomed Opt Express 5 (4) (2014) 1250–1261. https://doi.org/10.1364/BOE.5.001250.